Cavity QED engineering of spin dynamics in a spinor gas

Scott Parkins

Dodd-Walls Centre for Photonic and Quantum Technologies,
Department of Physics, University of Auckland

3 April 2019

DODD-WALLS CENTRE
for Photonic and Quantum Technologies

Outline

1. Spinor BECs and dynamics
2. Spinor Dicke Model
3. Cavity QED engineering of spinor dynamics
4. Spin-nematic squeezing
5. Many-Body Entanglement via Cavity Output Photon Counting
6. Multiphoton Pulses from a Single Spin-F Atom
7. Some other recent work

Outline

1. Spinor BECs and dynamics
2. Spinor Dicke Model
3. Cavity QED engineering of spinor dynamics
4. Spin-nematic squeezing
5. Many-Body Entanglement via Cavity Output Photon Counting
6. Multiphoton Pulses from a Single Spin-F Atom
7. Some other recent work

Spinor Bose gases

- Spinor Bose-Einstein Condensates (BECs): atoms in all magnetic sublevels of a single hyperfine ground state (e.g., $F = 1$ of $^{87}\mathrm{Rb}$) condensed
- Ensembles of integer-spin particles
- Vast array of phenomena possible related to magnetism, superfluidity, many-body quantum dynamics, ...

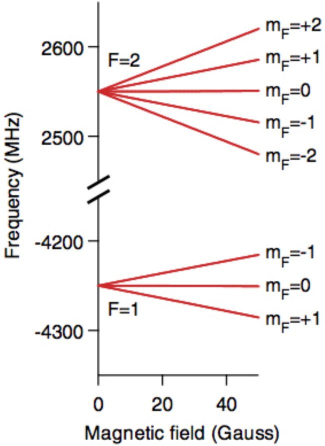

Kawaguchi & Ueda, Physics Reports **520**, 253 (2012)
Stamper-Kurn & Ueda, Rev. Mod. Phys. **85**, 1191 (2013)

Spinor Bose gases

- Small, tightly confined condensates
  $\Rightarrow$ all atoms have same spatial wave function
  $\Rightarrow$ single mode approximation

  Collisional spin dynamics described by

$$\hat{H} = \lambda \hat{\mathbf{J}}^2 \ , \qquad \hat{\mathbf{J}} = (\hat{J}_x, \hat{J}_y, \hat{J}_z) = \text{total spin vector}$$

  $\lambda =$ collisional spin interaction energy per particle integrated over condensate

  Law, Pu & Bigelow, Phys. Rev. Lett. **81**, 5257 (1998)

- Spinor dynamical rate $c = 2N\lambda \sim 10$ Hz
  for $N \sim 40,000$ ^{87}Rb atoms

Spinor Bose gases

- Add a magnetic field

$$\hat{H} = \lambda \hat{\mathbf{J}}^2 + p\hat{J}_z + q\hat{N}_0$$

  - linear Zeeman shift $\propto p$
  - quadratic Zeeman shift $\propto q$ (population N_0 in $m = 0$)

- Rich phase diagram & phenomena as a function of q/c

- Studies of
  - coherent spin-mixing oscillations and instabilities
  - dynamics of systems near quantum phase transitions
  - symmetry breaking in closed quantum systems
  - generation of correlated quantum spin states (of practical use for metrology)

Our motivation

- Can we use interactions in cavity QED to emulate and possibly extend this physics?
- If so, this could give us access to the rich physics of spinor BECs, without the actual need for BEC, but also with more flexibility and new possibilities for manipulation and measurement.

Outline

1. Spinor BECs and dynamics
2. Spinor Dicke Model
3. Cavity QED engineering of spinor dynamics
4. Spin-nematic squeezing
5. Many-Body Entanglement via Cavity Output Photon Counting
6. Multiphoton Pulses from a Single Spin-F Atom
7. Some other recent work

- Ensemble of tightly-confined atoms inside an optical cavity
- Lasers & cavity mode drive Raman transitions between m_F states
- Cavity mode mediates long-range interactions between atoms

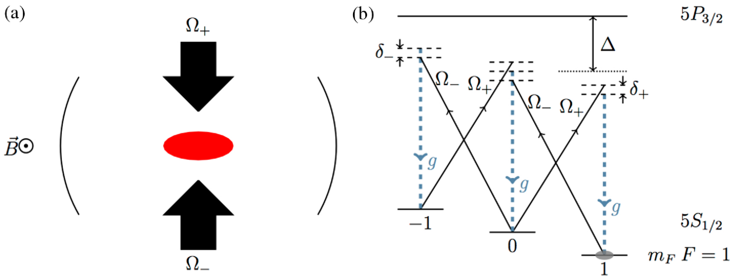

Zhiqiang et al., Optica **4**, 424 (2017)

Spinor Dicke Model: Theory

- Atoms in $F = 1$ hyperfine level
- Cavity/laser fields detuned from atomic resonance
- Effective atom-cavity model with spin-1 atoms

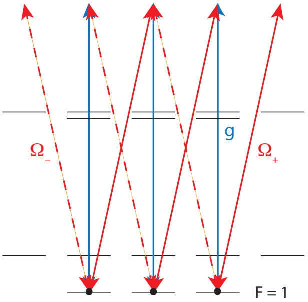

Spinor Dicke Model: Theory

- Atoms in $F = 1$ hyperfine level
- Cavity/laser fields detuned from atomic resonance
- Effective atom-cavity model with spin-1 atoms

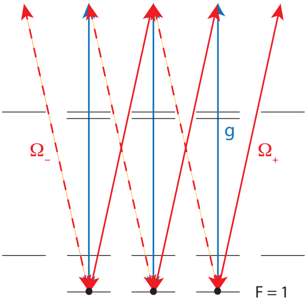

$$
\begin{aligned}
H = \; & \omega a^\dagger a + \omega_0 J_z + \omega_q Q_{zz} + (\delta_q/2N) Q_{zz} a^\dagger a + h(Q_{xx} - Q_{yy}) \\
& + \frac{\lambda_-}{\sqrt{2N}} \left(a J_+ + a^\dagger J_- \right) + \frac{\lambda_+}{\sqrt{2N}} \left(a^\dagger J_+ + a J_- \right) \\
& + \frac{\xi_x}{\sqrt{2N}} Q_{xz} \left(a^\dagger + a \right) + \frac{i\xi_y}{\sqrt{2N}} Q_{yz} \left(a^\dagger - a \right)
\end{aligned}
$$

Note: $Q_{ij} = \sum_{n=1}^{N} S_i^{(n)} S_j^{(n)} + S_j^{(n)} S_i^{(n)} - (4/3)\delta_{ij}$, $\{i,j\} \in \{x,y,z\}$

Spinor Dicke Model: Theory

- Cavity/laser fields very far detuned from atomic resonance
- Effective Dicke or Tavis-Cummings model with spin-1 (or spin-F) atoms

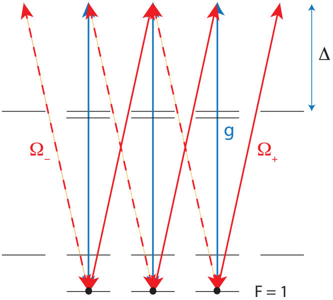

$$H = \omega a^\dagger a + \omega_0 J_z + \frac{\lambda_-}{\sqrt{2N}}\left(aJ_+ + a^\dagger J_-\right) + \frac{\lambda_+}{\sqrt{2N}}\left(a^\dagger J_+ + aJ_-\right)$$

$$\omega = \omega_{\rm c} - \frac{1}{2}(\omega_- + \omega_+) + \frac{Ng^2}{3\Delta}, \qquad \lambda_\pm = \frac{\sqrt{N}g\Omega_\pm}{12\Delta}$$

$$\omega_0 = \omega_{\rm Z} - \frac{1}{2}(\omega_- - \omega_+) + \frac{1}{24}\left(\frac{\Omega_-^2}{\Delta} - \frac{\Omega_+^2}{\Delta}\right)$$

Demonstration: Nonequilibrium phase transition in a spin-1 Dicke model

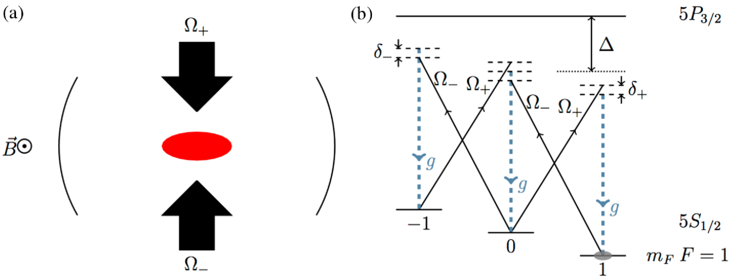

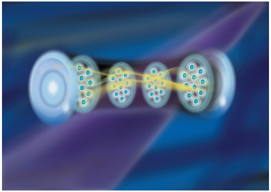

Zhiqiang et al., Optica **4**, 424 (2017)
(CQT Singapore)

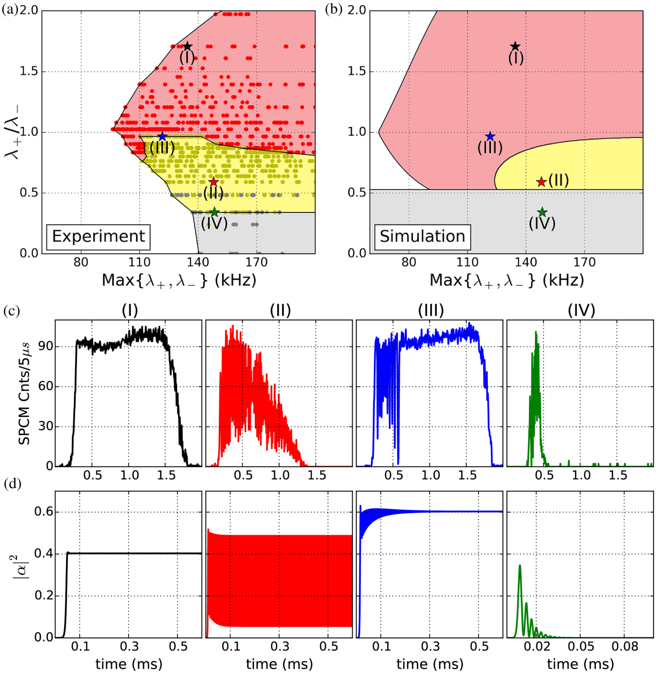

(a)
Experiment
(I)
(II)
(III)
(IV)
λ_+/λ_-
Max$\{\lambda_+,\lambda_-\}$ (kHz)
(b)
Simulation
(c)
SPCM Cnts/5μs
(d)
$|\alpha|^2$
time (ms)

Side Note: Nonlinear semiclassical dynamics in the unbalanced, open Dicke model

- Evidence of oscillatory phase in experiment

Side Note: Nonlinear semiclassical dynamics in the unbalanced, open Dicke model

- Evidence of oscillatory phase in experiment
- Detailed analysis of semiclassical dynamics reveals much,

Side Note: Nonlinear semiclassical dynamics in the unbalanced, open Dicke model

- Evidence of oscillatory phase in experiment
- Detailed analysis of semiclassical dynamics reveals much, **much more** ...

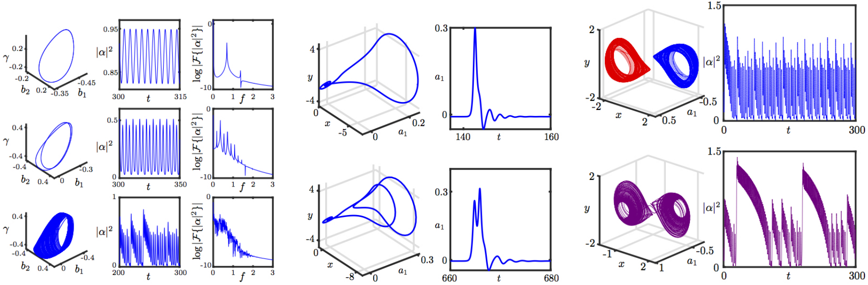

Kevin Stitely, Andrus Giraldo, Bernd Krauskopf, SP, in preparation

Side Note: Nonlinear semiclassical dynamics in the unbalanced, open Dicke model

Master equation model:

$$\dot{\rho} = -i[H,\rho] + \kappa\left(2a\rho a^\dagger - a^\dagger a\rho - \rho a^\dagger a\right)$$
$$H = \omega a^\dagger a + \omega_0 J_z + \frac{\lambda_-}{\sqrt{2N}}\left(aJ_+ + a^\dagger J_-\right) + \frac{\lambda_+}{\sqrt{2N}}\left(a^\dagger J_+ + aJ_-\right)$$

Define $\quad \alpha = \dfrac{\langle a\rangle}{\sqrt{2N}}, \quad \beta = \dfrac{\langle J_-\rangle}{2N}, \quad \gamma = \dfrac{\langle J_z\rangle}{2N}$

Nonlinear semiclassical equations of motion

$$\dot{\alpha} = -(\kappa + i\omega)\alpha - i\lambda_-\beta - i\lambda_+\beta^*$$
$$\dot{\beta} = -i\omega_0\beta + 2i\lambda_-\alpha\gamma + 2i\lambda_+\alpha^*\gamma$$
$$\dot{\gamma} = i\lambda_-\left(\alpha^*\beta - \alpha\beta^*\right) + i\lambda_+\left(\alpha\beta - \alpha^*\beta^*\right)$$

Side Note: Nonlinear semiclassical dynamics in the unbalanced, open Dicke model

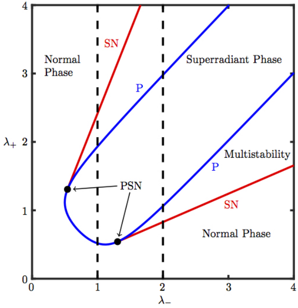

FIG. 3. Two parameter bifurcation diagram describing the superradiant phase transition, λ_- and λ_+. The red curves (SN) outline the locations of the saddle-node bifurcations and the blue curve (P) outlines the locations of the pitchfork bifurcations. Degenerate pitchfork-saddle-node bifurcations are shown as black dots and labelled PSN. The vertical dashed lines indicate the slices of the parameter plane that produce Fig. 2, above and below, respectively. Other parameters are set at $\kappa = \omega = \omega_0 = 1$.

Side Note: Nonlinear semiclassical dynamics in the unbalanced, open Dicke model

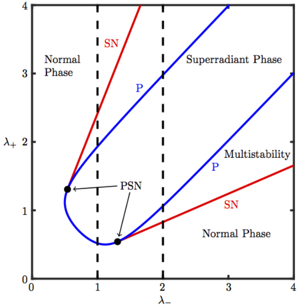

FIG. 3. Two parameter bifurcation diagram describing the superradiant phase transition, λ_- and λ_+. The red curves (SN) outline the locations of the saddle-node bifurcations and the blue curve (P) outlines the locations of the pitchfork bifurcations. Degenerate pitchfork-saddle-node bifurcations are shown as black dots and labelled PSN. The vertical dashed lines indicate the slices of the parameter plane that produce Fig. 2, above and below, respectively. Other parameters are set at $\kappa = \omega = \omega_0 = 1$.

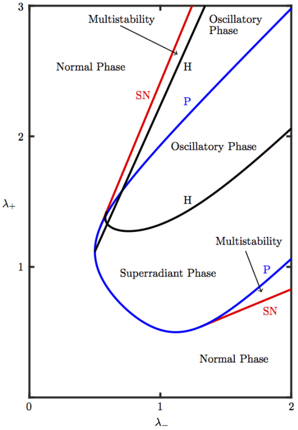

FIG. 8. Oscillatory phase diagram in two parameters. Locations of Hopf bifurcations are given by the black solid and dashed curves (H). The region bounded by the two curves details the oscillatory phase. Here $\kappa = \omega = \omega_0 = 1$.

Side Note: Nonlinear semiclassical dynamics in the unbalanced, open Dicke model

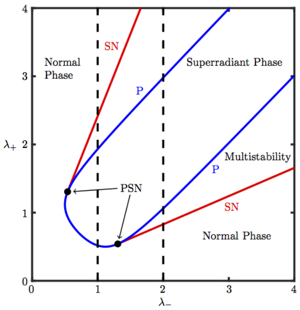

FIG. 3. Two parameter bifurcation diagram describing the superradiant phase transition, λ_- and λ_+. The red curves (SN) outline the locations of the saddle-node bifurcations and the blue curve (P) outlines the locations of the pitchfork bifurcations. Degenerate pitchfork-saddle-node bifurcations are shown as black dots and labelled PSN. The vertical dashed lines indicate the slices of the parameter plane that produce Fig. 2, above and below, respectively. Other parameters are set at $\kappa = \omega = \omega_0 = 1$.

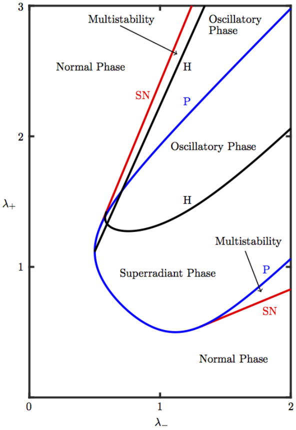

FIG. 8. Oscillatory phase diagram in two parameters. Locations of Hopf bifurcations are given by the black solid and dashed curves (H). The region bounded by the two curves details the oscillatory phase. Here $\kappa = \omega = \omega_0 = 1$.

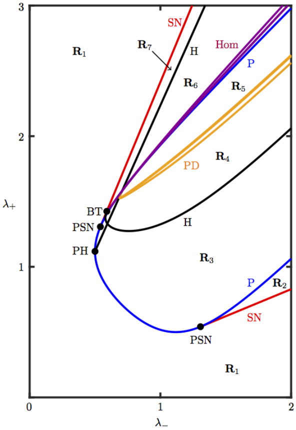

FIG. 16. Phase diagram with homoclinic bifurcation curves. Depicted are curves of saddle-node bifurcations (SN), pitchfork bifurcations (P), Hopf bifurcations (H), period-doubling bifurcations (PD), and Shil'nikov-type homoclinic bifurcations (Hom). These bifurcations divide the parameter plane (λ_-, λ_+) into regions $\mathbf{R}_i$, $i = 1, \cdots, 7$.

Outline

1. Spinor BECs and dynamics
2. Spinor Dicke Model
3. Cavity QED engineering of spinor dynamics
4. Spin-nematic squeezing
5. Many-Body Entanglement via Cavity Output Photon Counting
6. Multiphoton Pulses from a Single Spin-F Atom
7. Some other recent work

Dispersive limit of the spin-1 Dicke mode

- Now consider the dispersive limit in which the Raman transitions are themselves off-resonant, i.e., $\omega \gg \omega_0, \lambda_\pm$

Dispersive limit of the spin-1 Dicke mode

- Now consider the dispersive limit in which the Raman transitions are themselves off-resonant, i.e., $\omega \gg \omega_0, \lambda_\pm$
- Adiabatically eliminate the cavity mode to yield the reduced master equation

$$\dot{\rho} = -i[\hat{H}, \rho] + \frac{\kappa}{2N(\omega^2 + \kappa^2)} \mathcal{D}[\lambda_- \hat{J}_- + \lambda_+ \hat{J}_+]\rho$$

where $\mathcal{D}[O]\rho = 2O\rho O^\dagger - O^\dagger O\rho - \rho O^\dagger O$ and

$$\begin{aligned} \hat{H} = & \left[\omega_0 - \frac{\omega(\lambda_-^2 - \lambda_+^2)}{2N(\omega^2 + \kappa^2)}\right] \hat{J}_z \\ & - \frac{\omega}{2N(\omega^2 + \kappa^2)} \left[(\lambda_- + \lambda_+)^2 \hat{J}_x^2 + (\lambda_- - \lambda_+)^2 \hat{J}_y^2\right]. \end{aligned}$$

Dispersive limit of the spin-1 Dicke mode

- Set $\lambda_+ = 0$ and $\lambda_- = \lambda$ then

$$\dot{\rho} = -i[\hat{H}, \rho] + \frac{\Gamma}{2N}\mathcal{D}[\hat{J}_-]\rho$$

where

$$\hat{H} = \omega_0' \hat{J}_z + \frac{\Lambda}{2N}(\hat{J}_x^2 + \hat{J}_y^2)$$

with

$$\omega_0' = \omega_0 + \frac{\Lambda}{2N}, \quad \Lambda = -\frac{\omega\lambda^2}{\omega^2 + \kappa^2}, \quad \Gamma = -\frac{\kappa}{\omega}\Lambda$$

Simulation of spinor physics

$$\dot{\rho} = -i[\hat{H}, \rho] + \frac{\Gamma}{2N}\mathcal{D}[\hat{J}_-]\rho \ , \qquad \hat{H} = \omega_0' \hat{J}_z + \frac{\Lambda}{2N}(\hat{J}_x^2 + \hat{J}_y^2)$$

$$\omega_0' = \omega_0 + \frac{\Lambda}{2N}, \quad \Lambda = -\frac{\omega\lambda^2}{\omega^2 + \kappa^2}, \quad \Gamma = -\frac{\kappa}{\omega}\Lambda$$

Simulation of spinor physics

$$\dot{\rho} = -i[\hat{H}, \rho] + \frac{\Gamma}{2N}\mathcal{D}[\hat{J}_-]\rho \ , \qquad \hat{H} = \omega_0' \hat{J}_z + \frac{\Lambda}{2N}(\hat{J}_x^2 + \hat{J}_y^2)$$

$$\omega_0' = \omega_0 + \frac{\Lambda}{2N}, \quad \Lambda = -\frac{\omega\lambda^2}{\omega^2 + \kappa^2}, \quad \Gamma = -\frac{\kappa}{\omega}\Lambda$$

- Emulates spinor dynamics for conserved J_z and $\Gamma/\Lambda \ll 1$

Simulation of spinor physics

$$\dot{\rho} = -i[\hat{H}, \rho] + \frac{\Gamma}{2N}\mathcal{D}[\hat{J}_-]\rho \ , \qquad \hat{H} = \omega_0'\hat{J}_z + \frac{\Lambda}{2N}(\hat{J}_x^2 + \hat{J}_y^2)$$

$$\omega_0' = \omega_0 + \frac{\Lambda}{2N}, \quad \Lambda = -\frac{\omega\lambda^2}{\omega^2 + \kappa^2}, \quad \Gamma = -\frac{\kappa}{\omega}\Lambda$$

- Emulates spinor dynamics for conserved J_z and $\Gamma/\Lambda \ll 1$
- Ferromagnetic or anti-ferromagnetic interactions chosen by sign of ω (Raman detuning)

Simulation of spinor physics

$$\dot{\rho} = -i[\hat{H}, \rho] + \frac{\Gamma}{2N}\mathcal{D}[\hat{J}_-]\rho \ , \qquad \hat{H} = \omega_0' \hat{J}_z + \frac{\Lambda}{2N}(\hat{J}_x^2 + \hat{J}_y^2)$$

$$\omega_0' = \omega_0 + \frac{\Lambda}{2N}, \quad \Lambda = -\frac{\omega\lambda^2}{\omega^2 + \kappa^2}, \quad \Gamma = -\frac{\kappa}{\omega}\Lambda$$

- Emulates spinor dynamics for conserved J_z and $\Gamma/\Lambda \ll 1$
- Ferromagnetic or anti-ferromagnetic interactions chosen by sign of ω (Raman detuning)
- Artificial quadratic Zeeman shift possible with, e.g., additional, weak π-polarised laser

Simulation of spinor physics

$$\dot{\rho} = -i[\hat{H}, \rho] + \frac{\Gamma}{2N}\mathcal{D}[\hat{J}_-]\rho \ , \qquad \hat{H} = \omega_0' \hat{J}_z + \frac{\Lambda}{2N}(\hat{J}_x^2 + \hat{J}_y^2)$$

$$\omega_0' = \omega_0 + \frac{\Lambda}{2N}, \quad \Lambda = -\frac{\omega\lambda^2}{\omega^2 + \kappa^2}, \quad \Gamma = -\frac{\kappa}{\omega}\Lambda$$

- Emulates spinor dynamics for conserved J_z and $\Gamma/\Lambda \ll 1$
- Ferromagnetic or anti-ferromagnetic interactions chosen by sign of ω (Raman detuning)
- Artificial quadratic Zeeman shift possible with, e.g., additional, weak π-polarised laser
- Spin-1,2,3,4, ... possible ($^{87}\mathrm{Rb}$, $^{85}\mathrm{Rb}$, $^{133}\mathrm{Cs}$, ...)

Simulation of spinor physics

$$\dot{\rho} = -i[\hat{H}, \rho] + \frac{\Gamma}{2N}\mathcal{D}[\hat{J}_-]\rho \ , \qquad \hat{H} = \omega_0' \hat{J}_z + \frac{\Lambda}{2N}(\hat{J}_x^2 + \hat{J}_y^2)$$

$$\omega_0' = \omega_0 + \frac{\Lambda}{2N}, \quad \Lambda = -\frac{\omega\lambda^2}{\omega^2 + \kappa^2}, \quad \Gamma = -\frac{\kappa}{\omega}\Lambda$$

- Emulates spinor dynamics for conserved J_z and $\Gamma/\Lambda \ll 1$
- Ferromagnetic or anti-ferromagnetic interactions chosen by sign of ω (Raman detuning)
- Artificial quadratic Zeeman shift possible with, e.g., additional, weak π-polarised laser
- Spin-1,2,3,4, ... possible ($^{87}\mathrm{Rb}$, $^{85}\mathrm{Rb}$, $^{133}\mathrm{Cs}$, ...)
- Dissipation-driven dynamics (reservoir engineering) possible for $\Gamma \gtrsim \Lambda$ (or $\Lambda = 0$)

Simulation of spinor physics

$$\dot{\rho} = -i[\hat{H}, \rho] + \frac{\Gamma}{2N}\mathcal{D}[\hat{J}_-]\rho \ , \qquad \hat{H} = \omega_0' \hat{J}_z + \frac{\Lambda}{2N}(\hat{J}_x^2 + \hat{J}_y^2)$$

$$\omega_0' = \omega_0 + \frac{\Lambda}{2N}, \quad \Lambda = -\frac{\omega\lambda^2}{\omega^2 + \kappa^2}, \quad \Gamma = -\frac{\kappa}{\omega}\Lambda$$

- Emulates spinor dynamics for conserved J_z and $\Gamma/\Lambda \ll 1$
- Ferromagnetic or anti-ferromagnetic interactions chosen by sign of ω (Raman detuning)
- Artificial quadratic Zeeman shift possible with, e.g., additional, weak π-polarised laser
- Spin-1,2,3,4, ... possible ($^{87}\mathrm{Rb}$, $^{85}\mathrm{Rb}$, $^{133}\mathrm{Cs}$, ...)
- Dissipation-driven dynamics (reservoir engineering) possible for $\Gamma \gtrsim \Lambda$ (or $\Lambda = 0$)
- Cavity output $\rightarrow$ "window" on dynamics, or measurement-induced state preparation

Simulation of spinor physics

- Dynamical rate set by Raman transition rates, light shifts and detunings

Simulation of spinor physics

- Dynamical rate set by Raman transition rates, light shifts and detunings
- Potentially orders of magnitude faster (than actual BECs):

  $\{g, \kappa, \gamma\}/(2\pi) = \{10, 0.2, 6\}$ MHz, $\quad N = 10^4$ atoms

  $\lambda/(2\pi) \simeq 200$ kHz, $\quad \omega/(2\pi) \simeq 4$ MHz

  $\rightarrow \Lambda/(2\pi) \simeq 10$ kHz, $\quad \Gamma/\Lambda = 0.05$

Simulation of spinor physics

- Dynamical rate set by Raman transition rates, light shifts and detunings
- Potentially orders of magnitude faster (than actual BECs):

  $\{g, \kappa, \gamma\}/(2\pi) = \{10, 0.2, 6\}$ MHz, $\quad N = 10^4$ atoms

  $\lambda/(2\pi) \simeq 200$ kHz, $\quad \omega/(2\pi) \simeq 4$ MHz

  $\rightarrow \Lambda/(2\pi) \simeq 10$ kHz, $\quad \Gamma/\Lambda = 0.05$

- Note: Minimise effects of atomic spontaneous emission with large single-atom cooperativity $C = 2g^2/(\kappa\gamma)$

S. Masson, M. Barrett, SP, Phys. Rev. Lett. **119**, 213601 (2017)

Outline

1. Spinor BECs and dynamics
2. Spinor Dicke Model
3. Cavity QED engineering of spinor dynamics
4. Spin-nematic squeezing
5. Many-Body Entanglement via Cavity Output Photon Counting
6. Multiphoton Pulses from a Single Spin-F Atom
7. Some other recent work

Spin-nematic squeezing

Spin-1 system:

$$\dot{\rho} = -i[H,\rho] + \frac{\Gamma}{2N}\mathcal{D}[J_-]\rho \ , \qquad H = \frac{\Lambda}{2N}(J_x^2 + J_y^2)$$

with initial atomic state $|0, N, 0\rangle$

Spin-nematic squeezing

Spin-1 system:

$$\dot{\rho} = -i[H,\rho] + \frac{\Gamma}{2N}\mathcal{D}[J_-]\rho\ , \qquad H = \frac{\Lambda}{2N}(J_x^2 + J_y^2)$$

with initial atomic state $|0, N, 0\rangle$

Bosonic mode representation: $J_- = \sqrt{2}(a_0^\dagger a_1 + a_{-1}^\dagger a_0)$

$$H \sim a_0^\dagger a_0^\dagger a_{-1} a_{+1} + a_{-1}^\dagger a_{+1}^\dagger a_0 a_0$$

Spin-nematic squeezing

Spin-1 system:

$$\dot{\rho} = -i[H,\rho] + \frac{\Gamma}{2N}\mathcal{D}[J_-]\rho \ , \qquad H = \frac{\Lambda}{2N}(J_x^2 + J_y^2)$$

with initial atomic state $|0, N, 0\rangle$

Bosonic mode representation: $J_- = \sqrt{2}(a_0^\dagger a_1 + a_{-1}^\dagger a_0)$

$$H \sim a_0^\dagger a_0^\dagger a_{-1} a_{+1} + a_{-1}^\dagger a_{+1}^\dagger a_0 a_0$$

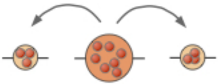

Spin-nematic squeezing $\rightarrow$ redistribution of quantum noise in the subspace $\{S_x, Q_{yz}, Q_{zz} - Q_{yy}\}$: quantify with

$$\xi_x^2 = \frac{\langle[\Delta(\cos\theta\, J_x + \sin\theta\, Q_{yz})]^2\rangle}{\langle Q_{zz} - Q_{yy}\rangle/2} < 1 \quad \text{for squeezing}$$

Spin-nematic squeezing

ξ_x^2 vs time and phase for $\Gamma/\Lambda = 0.05$

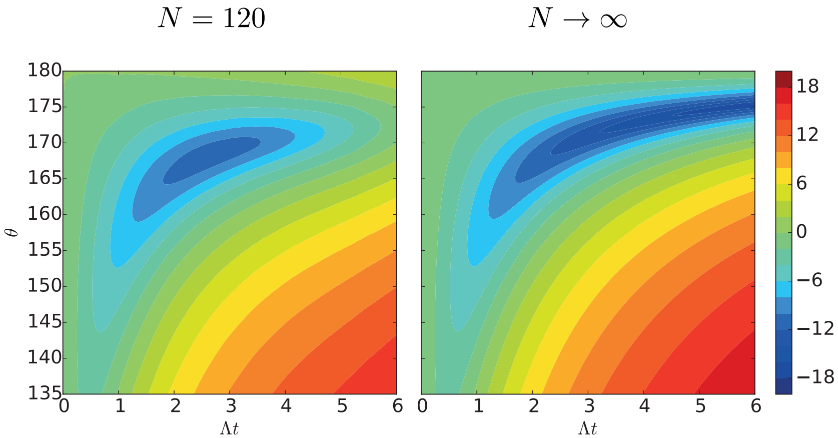

- $N \to \infty$: set $a_0 = \sqrt{N}$

$$\xi_x^2 = (\cos\theta + 2\Lambda t \sin\theta)^2 + (1 + 2\Gamma t)^2 \sin^2\theta$$

Best ξ_x^2 vs N

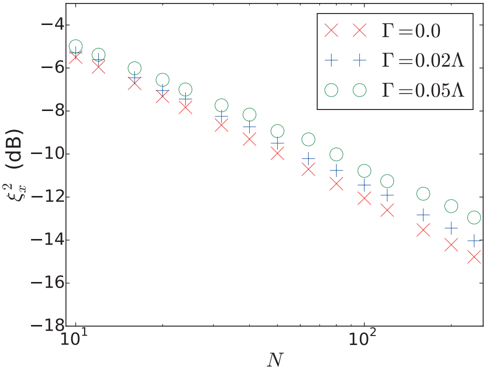

$$(\xi_x^2)_{\rm opt} \sim N^{-0.67}$$

S. Masson, M. Barrett, SP, Phys. Rev. Lett. **119**, 213601 (2017)

Note:
Recent demonstration of cavity-mediated "pair creation" process

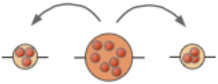

Davis et al., Phys. Rev. Lett. **122**, 010405 (2019)
(Schleier-Smith group, Stanford)

Outline

1 Spinor BECs and dynamics

2 Spinor Dicke Model

3 Cavity QED engineering of spinor dynamics

4 Spin-nematic squeezing

5 Many-Body Entanglement via Cavity Output Photon Counting

6 Multiphoton Pulses from a Single Spin-F Atom

7 Some other recent work

- N spin-1 atoms
- Initial atomic state $|m_F = 0\rangle^{\otimes N} \equiv \sum_{J=0}^{N} c_J |J, 0\rangle$
(uncertain total spin length)

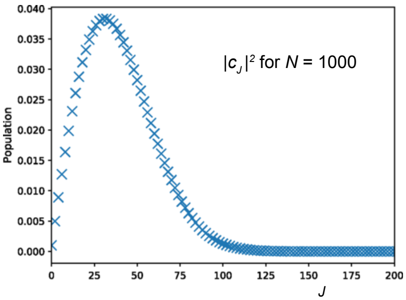

- $|c_J|^2$ centred around $J \simeq \sqrt{N}$
- All states $|S, 0\rangle$ with $S < N$ are entangled

Many-Body Entanglement via Photon Counting

Evolution with effective Tavis-Cummings model ($\lambda_+ = 0$):

$$\dot{\rho} = -i[H, \rho] + \kappa \left(2a\rho a^\dagger - a^\dagger a \rho - \rho a^\dagger a \right), \quad H = \lambda_- \left(aJ_+ + a^\dagger J_- \right)$$

$$\sum_{J=0}^{N} c_J |J, 0\rangle \otimes |0\rangle_{\rm cav} \longrightarrow \sum_{J=0}^{N} c_J |J, -J\rangle \otimes |0\rangle_{\rm cav} \otimes |J\rangle_{\rm out}$$

where

$|J\rangle_{\rm out}$ = J-photon output pulse from the cavity

- Ideal photon counting measurement projects spin state onto particular entangled state $|J, -J\rangle$
  (probability of $J = N$ negligible for $N \gg 1$)

Many-Body Entanglement via Photon Counting

- Can quantify metrological sensitivity of a quantum state by *quantum Fisher information* $\mathcal{F}$.
- Variance of measured phase θ imprinted by a classical parameter is bounded by $(\Delta\theta)^2 \geq \mathcal{F}^{-1}$.
- Optimal classical state: $\mathcal{F} \sim N$
  Heisenberg limit: $\mathcal{F} \sim N^2$
- For pure states, the QFI over a generator $\hat{G}$ is $\mathcal{F} = 4(\Delta\hat{G})^2$.

Many-Body Entanglement via Photon Counting

- Can quantify metrological sensitivity of a quantum state by *quantum Fisher information* $\mathcal{F}$.
- Variance of measured phase θ imprinted by a classical parameter is bounded by $(\Delta\theta)^2 \geq \mathcal{F}^{-1}$.
- Optimal classical state: $\mathcal{F} \sim N$
  Heisenberg limit: $\mathcal{F} \sim N^2$
- For pure states, the QFI over a generator $\hat{G}$ is $\mathcal{F} = 4(\Delta\hat{G})^2$.

- We consider $\hat{G} = \hat{Q}_{xx} - \hat{Q}_{yy}$ $\qquad (\propto \hat{a}^\dagger_{+1}\hat{a}_{-1} + \hat{a}^\dagger_{-1}\hat{a}_{+1})$
- Average QFI of a single run (detection efficiency η):

$$\bar{\mathcal{F}}_{\eta=1} = \sum_{J=0}^{N} |c_J|^2 \mathcal{F}(|J,-J\rangle) \sim N^2$$

- Imperfect detection efficiency: e.g., $\bar{\mathcal{F}}_{\eta=0.5} \sim N^{1.6}$

Many-Body Entanglement via Photon Counting

- Imperfect detection efficiency: e.g., $\bar{\mathcal{F}}_{\eta=0.5} \sim N^{1.6}$
- **But**, switch laser polarisation to give anti-Tavis-Cummings model ($\lambda_- = 0, \lambda_+ \neq 0$), then

$$|J,-J\rangle \otimes |0\rangle_{\rm cav} \longrightarrow |J,+J\rangle \otimes |0\rangle_{\rm cav} \otimes |2J\rangle_{\rm out}$$

- Sequence of TC and anti-TC interactions $\rightarrow$ sequence of photon counting measurements $\rightarrow$ narrowing of distribution in J $\rightarrow$ recovery of Heisenberg scaling

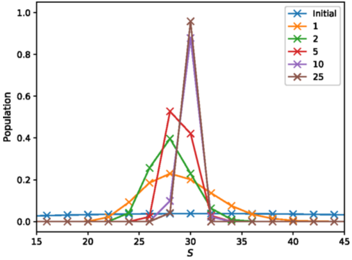

Stuart Masson, SP, Phys. Rev. Lett. **122**, 103601 (2019)

Outline

1. Spinor BECs and dynamics
2. Spinor Dicke Model
3. Cavity QED engineering of spinor dynamics
4. Spin-nematic squeezing
5. Many-Body Entanglement via Cavity Output Photon Counting
6. Multiphoton Pulses from a Single Spin-F Atom
7. Some other recent work

- One spin-F atom coupled to a nanocavity ...

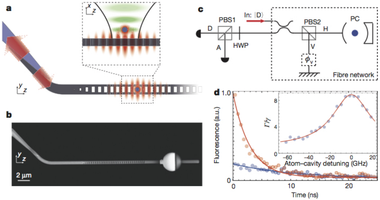

$g \gtrsim 2\pi \cdot 1$ GHz

Tiecke et al, Nature **508**, 242 (2014)

- ... or to a fibre Fabry-Pérot microcavity

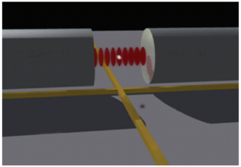

$g \gtrsim 2\pi \cdot 200$ MHz

G. Barontini et al., Science **349**, 1317 (2015)

Multiphoton Pulses from a Single Atom

Single-atom effective Tavis-Cummings model ($\lambda_+ = 0$):

$$\dot{\rho} = -i[H,\rho] + \kappa\left(2a\rho a^\dagger - a^\dagger a\rho - \rho a^\dagger a\right), \quad H = \lambda_-\left(aJ_+ + a^\dagger J_-\right)$$

$$|J,+J\rangle \otimes |0\rangle_{\text{cav}} \longrightarrow |J,-J\rangle \otimes |0\rangle_{\text{cav}} \otimes |2J\rangle_{\text{out}}$$

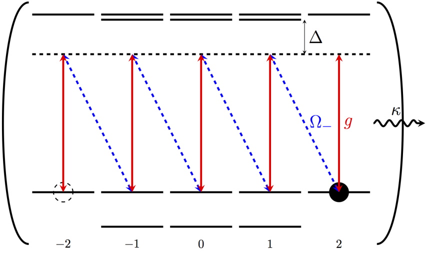

Multiphoton Pulses from a Single Atom

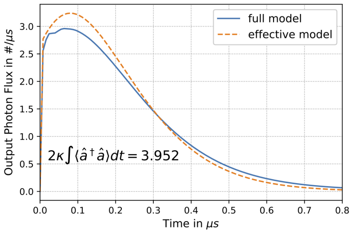

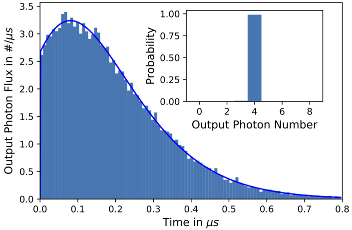

Caspar Groiseau, Stuart Masson, Alex Elliott, SP, in preparation

- $J = 2 \Rightarrow$ 4-photon "superradiant" pulse
- Initial superposition state:

$$\frac{|2,2\rangle + |2,-2\rangle}{\sqrt{2}} \otimes |0\rangle_{\text{out}}$$

$$\rightarrow |2,-2\rangle \otimes \frac{|0\rangle_{\text{out}} + |4\rangle_{\text{out}}}{\sqrt{2}}$$

- Homodyne tomography

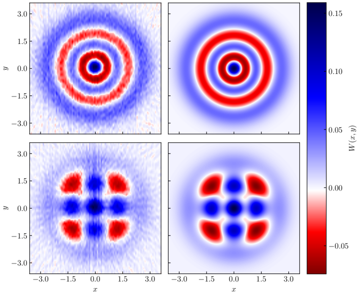

Outline

1 Spinor BECs and dynamics
2 Spinor Dicke Model
3 Cavity QED engineering of spinor dynamics
4 Spin-nematic squeezing
5 Many-Body Entanglement via Cavity Output Photon Counting
6 Multiphoton Pulses from a Single Spin-F Atom
7 Some other recent work

Coupled-cavities quantum electrodynamics: observation of dressed states of atoms with delocalised photons

Experiment at Waseda University, Tokyo

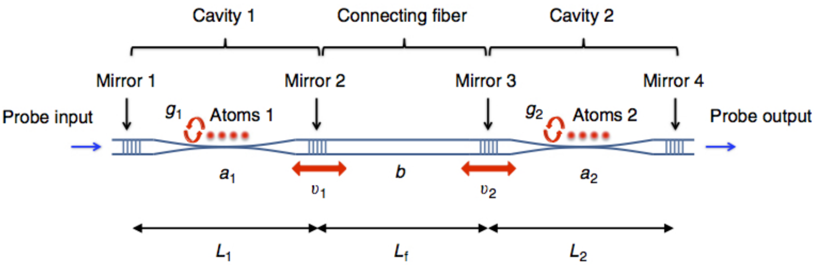

Shinya Kato, **Nikolett Német**, Kohei Senga, Shota Mizukami, Xinhe Huang, **SP**, Takao Aoki, Nat. Commun. **10**, 1038 (2019)

Weak driving: coupled oscillators

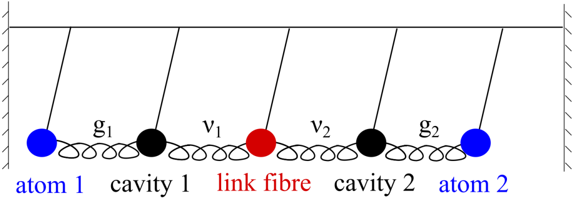

Normal modes:

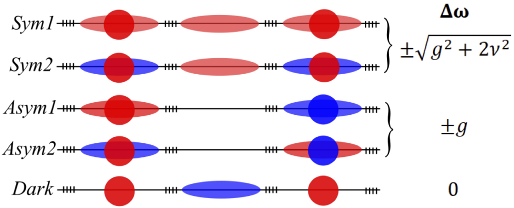

Weak field transmission spectra

Atoms separated by $>$ 1 metre strongly coupled via fibre-dark normal mode ...

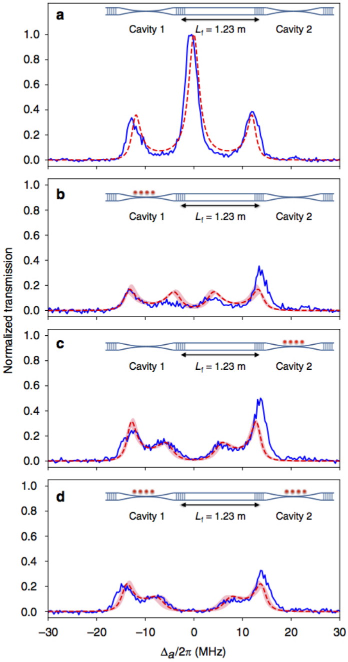

... or via cavity-dark normal mode

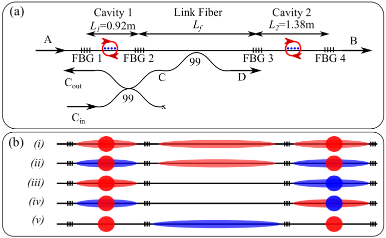

Donald White, Shinya Kato, **Nikolett Német**, **SP**, Takao Aoki, submitted